Experimental Determination of the Dependence Between Spectral Response and Current–Voltage Characteristics for MWIR HgCdTe Detectors

A. Kowalewski[1] · P. Madejczyk[1] · T. Manyk[1] · J. Rutkowski[1] · P. Martyniuk[1]

Abstract

Experimental results are reported for a medium-wavelength infrared (MWIR) HgCdTe photodetector designed in a joint laboratory run by VIGO Photonics S.A. and the Military University of Technology. The parameters of the MWIR detectors fabricated with HgCdTe heterostructures were studied. Advances in the metal–organic chemical vapor deposition (MOCVD) technique enable the growth of HgCdTe epilayers with a wide range of composition and doping, used for uncooled infrared detectors. Device-quality HgCdTe heterostructures were deposited on 2-inch-diameter, low-cost (100) GaAs substrates. The heterostructures obtained were examined measuring the spectral response and current–voltage characteristics in different temperatures. Our intention here was to determine the relationship between electrical and optical results, using thermal analysis of dark current properties and photocurrent and spectral characteristics. The appearance of an additional signal source in certain ranges of reverse voltages was examined. Comparative analysis of the electrical and electro-optical characterization enabled us to isolate the photocurrent originating from different layers of the detector structure. Automated measurement techniques make it possible to correlate current responsivity with current–voltage curves measured as a function of temperature in a range from 10 K to 300 K with ±0.05 K resolution without human exertion. LabVIEW-aided data acquisition enables the averaging of each characteristic several hundred times, eliminates random and human errors, and decreases measurement uncertainty.

✉ P. Madejczyk
pawel.madejczyk@wat.edu.pl

[1] Institute of Applied Physics, Military University of Technology, 2 gen. Kaliskiego St., 00-908 Warsaw, Poland

Graphical Abstract
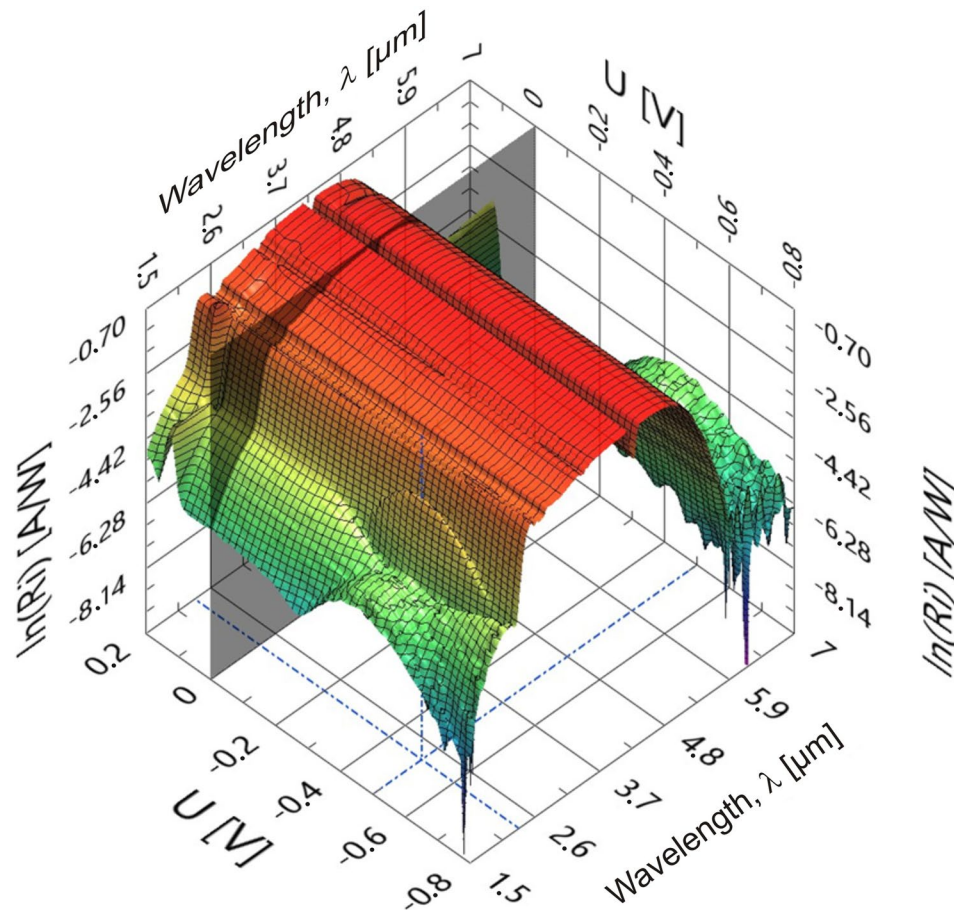
Keywords MOCVD · HgCdTe · spectral response · current–voltage characteristic · infrared detectors

Introduction

Many branches of science and industry require detectors operating in the infrared (IR) range (1–30 μm). Advances in IR detector technology have been mainly associated with photon detectors, among which photodiodes are typically the most sensitive devices. They are characterized by both a high signal-to-noise ratio and a fast response.[1] In spite of other competitive technologies and materials, mercury cadmium telluride (HgCdTe) is still the main material used for infrared detectors.[2] The development of advanced epitaxial techniques such as molecular beam epitaxy (MBE) and metal–organic chemical vapor deposition (MOCVD) allows for the construction of complex HgCdTe heterostructure-based IR detectors.[3–5] The high cost of CdZnTe substrates and their relatively small available area necessitate the search for alternative substrates for HgCdTe.[6] One attractive alternative is GaAs substrates, which are easily available in high-quality and large-area wafers.[7] The drawback here is the lattice mismatch of 14% between HgCdTe and GaAs, requiring the deposition of thick CdTe buffers.[8] Advances in IR detectors are also closely related to advanced characterization techniques that use high-precision source meters, fast signal analyzers, Fourier transform infrared (FTIR) spectrometers, low-noise amplifiers, and stable-temperature cryostats. When all these modern electronic devices are computer-controlled with the support of an automated programming environment (e.g. LabVIEW platform), detection ability enters a higher level. The possibility of multiple averaging decreases the measurement uncertainty, human error is reduced, research is faster, multiplied, and the results can be automatically processed, archived and analyzed.

Experiment

Materials

HgCdTe epitaxial growth was carried out in the horizontal reactor of an Aixtron AIX 200 MOCVD unit. Dimethyl-cadmium (DMCd) and diisopropyl telluride (DIPTe) were used as precursors. Ethyl iodine (EI) was used as a donor and tris(dimethylamino)arsenic (TDMAAs) as an acceptor of dopant sources. The growth was carried out on 2-inch, epi-ready, semi-insulating (100) GaAs substrates, oriented 2° off toward the nearest <110>. Typically, a 3–4-µm-thick CdTe layer is used as a buffer layer, reducing stress caused by crystal lattice misfit between the GaAs substrate and HgCdTe epitaxial layer structure.[9] The (111)B growth was enforced by a suitable nucleation procedure based on GaAs substrate annealing in a Te-rich atmosphere prior to the growth of the CdTe buffer.[10] The interdiffused multi-layer process (IMP) technique was applied for the HgCdTe deposition.[11] HgCdTe epilayers were grown at 350°C, with the mercury source maintained at 200°C. The II/VI mole ratio was kept in the range of 1.5–5 during CdTe cycles of the IMP process. Acceptor and donor doping was investigated over a wide concentration range, and doping levels of 5×10^{14} cm$^{to\ 3}$ to 5×10^{17} cm^{-3} were obtained. The obtained heterostructures were not annealed ex situ.[12] The growth of the HgCdTe epilayers with (111)B orientation has advantages such as a lack of large macro-defects and high growth rate; however, there are some disadvantages including rough surface morphology, a high concentration of residual background, and less efficient p-type doping. More comprehensive study of the growth process was described in Madejczyk et al.[13]

The structure chosen for the present study is a type of $n^+G_3P^+G_2pG_1N^+$. Looking at the structure from the substrate side, the first layer is N^+, which is a highly doped layer with $N_D > 10^{17}$ cm^{-3} to ensure low series resistance. The energy gap of the N^+ layer should be wider than that of the absorber region, since the structure is irradiated from the substrate side. Next, a graded gap region G_1 is placed between a wide-gap/highly donor-doped N^+ and narrow-gap/moderate acceptor-doped absorber. Diffusion processes at the growth temperature shape the energy gap profile. The medium-doped p-type absorber region is the central layer of the whole structure. Its doping level is higher than the donor-like background concentration, which is typically 3×10^{15} cm^{-3}. The absorber composition x corresponds to the expected cutoff wavelength of the detector. In this case, the composition of absorber x is $x = 0.32$, which ensures operation at the medium-wavelength infrared (MWIR) range. The thickness of an absorber layer is a compromise between requirements of high absorption and low thermal generation. In other words, it is the trade-off between quantum efficiency and R_0A product. Our experiments have allowed us to determine that the best results in terms of detectivity are obtained for absorbers with a thickness of about 4 µm. The graded gap G_2 region separates the wide-gap P^+ and narrow-gap absorber. The composition of the P^+ layer should be much larger than that of the absorber. The graded gap G_3 layer is located between P^+ and n^+. Finally, there is an n^+ contact layer on top with a donor concentration of about 10^{18} cm^{-3} for low resistance and a composition lower than that of the absorbing region. Information concerning the design and characterization of similar structures was reported by Gawron et al.[14] (Fig. 1).

The energy band gap diagram of the investigated device calculated by the SimuAPSYS (Crosslight Inc.) commercial platform is presented in Fig. 2. Calculations were performed under reverse voltage $U = -0.6$ V and temperature of 80 K. The regions of exemplary charge carrier generation are indicated, along with their possible flow directions. Note that the stream of photogenerated electrons originating at the G_3 region is opposite to the direction of electrons generated at other parts of the structure.

Figure 3 shows the secondary ion mass spectroscopy (SIMS) profile of the $n^+G_3P^+G_2pG_1N^+$ Hg$_{1-x}$Cd$_x$Te heterostructure with absorber composition $x = 0.32$. This is the profile of the real MOCVD-grown structure designed according to the assumptions as depicted in Fig. 1. The dashed black line represents the arsenic profile corresponding to abruptly changing doses of arsenic in successive layers p and P^+. The stable arsenic concentration in the absorber region with 6 cts/s corresponds to the expected acceptor level of 3×10^{15} cm^{-3}. There is no undesirable arsenic diffusion to the adjacent layers, so it is a stable dopant. The red line represents iodine counts of 8×10^2 and 2×10^2 in the n^+ and the N^+ regions, respectively, which correspond to the designed concentration levels 10^{18} cm^{-3} and 5×10^{17} cm^{-3}, respectively. Abrupt slopes are observed in the iodine profile. The tellurium, cadmium, and mercury counts enabled the calculation of a composition x profile (blue line) of the whole Hg$_{1-x}$Cd$_x$Te heterostructure. Wide-energy-gap N^+ and P^+ layers surround the narrower-gap absorber as assumed in the heterostructure project. Because of the interdiffusion processes in HgCdTe material during growth, a composition profile of the interfaces between the particular layers is graded. SIMS profile analysis enables changes to be made in the growth recipes and allows one to shape the expected profiles of detector structures.

Measurements

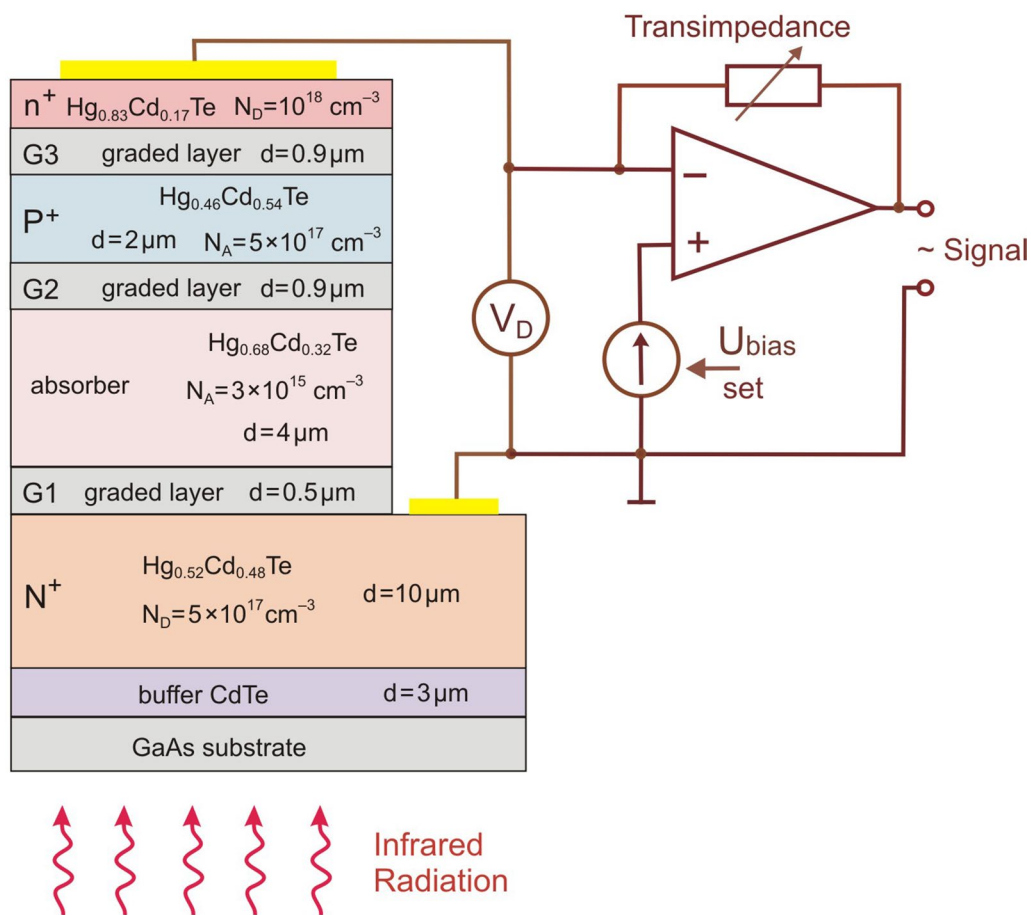The sample was attached to a holder and placed on a cold finger in a Janis helium cryostat. The sample holder permits

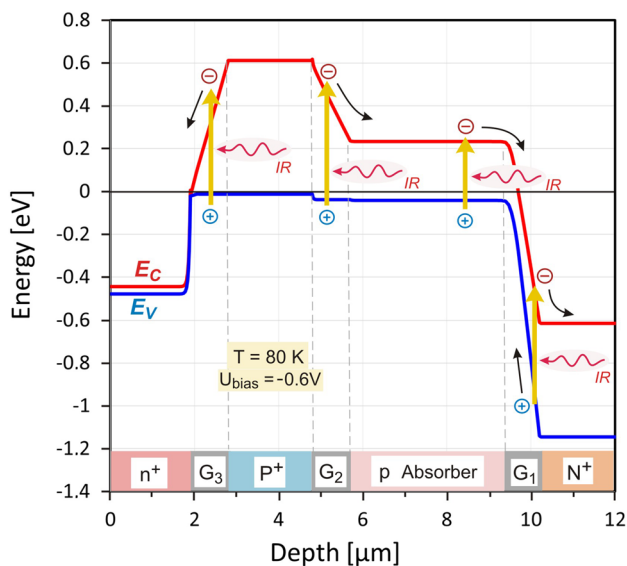**Fig. 1** The $n^+G_3P^+G_2pG_1N^+$ type MWIR HgCdTe heterostructure.

Fig. 2 The energy profile of the $n^+G_3P^+G_2pG_1N^+$ structure with exemplary charge carrier generation regions.
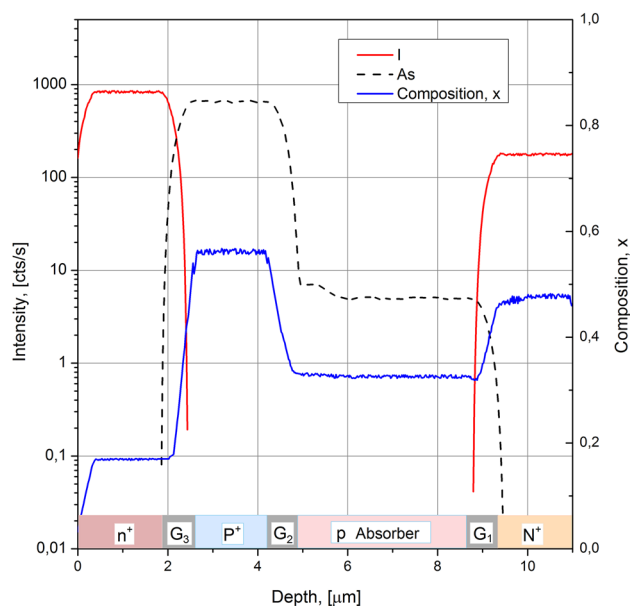

Fig. 3 SIMS profile of the MOCVD-grown $n^+G_3P^+G_2pG_1N^+$ HgCdTe heterostructure. Color figure online.

illumination of the sample with an external radiation source, and it can be completely shielded from background radiation through a cold shield for the dark current measurements. Temperature values were monitored by a sensor connected to a Lake Shore 335 controller. The temperature sensor was placed 10 mm from the sample at the same side of the cold finger. All data were collected in a stable temperature mode from 10 K to 300 K. All current–voltage characteristics were performed in the 2-contact mode using a Keysight B1500 multichannel programmable multi-meter. The sample was biased by a voltage source with simultaneous measurement of the current. The current–voltage characteristics were measured for a temperature range of 10 K to 300 K in 10 K steps. The *I–V* characteristics were measured at three different conditions. The first measurement set was the dark current as a function of voltage and is presented in Fig. 4a. Next, the sample was illuminated by an ambient background temperature of 300 K. From the current–voltage characteristics, we observe the influence of the background radiation in the form of additional photocurrent (Fig. 4b). For low temperatures ($T < 80$ K), the characteristic transition points (from positive to negative current values) move from a voltage $U = 0$ to the right (towards positive voltages). The third measurement set was performed with an additional illumination of the sample by the 1000 K blackbody.

Spectral responsivity was then measured keeping the same radiation density as during the illuminated *I–V* tests. A PerkinElmer FTIR spectrophotometer was used for this purpose. Measurements were made in a bias voltage range from +0.2 V to −1.4 V with a resolution of 0.02 V, for the same temperatures as current–voltage measurements. A current preamplifier (VIGO Photonics) was used to bias the detection structure. Figure 5 shows selected spectral characteristics taken at 80 K. This plot shows the bias voltage influence on the spectral characteristics. The basic

signal coming from the absorber layer with the composition $x = 0.32$ occurs at energy of 300 meV, and its position does not depend on the bias voltage. Significant changes in the signal as a function of voltage are visible in the energy range of 500–540 meV. In this range, the signal originating from the absorber is only about 20% of the maximum value at 300 meV. At bias voltages of −0.6 V (purple curve) and −0.8 V (yellow curve), the signal drops sharply above 500 meV, followed by a peak at 530 meV, which is the opposite of the proper absorber signal. For voltages below −1 V (blue curves and yellow-blue curve), a positive large signal appears at energy of 500 meV, exceeding the signal originating from the absorber at energy of 300 meV.
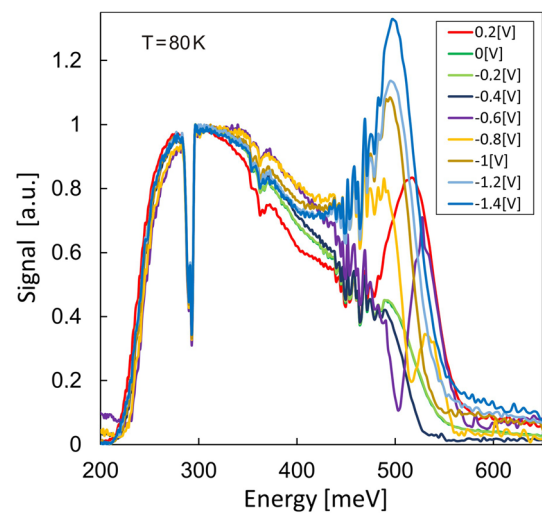
Fig. 5 Spectral response of the $n^+G_3P^+G_2pG_1N^+$ HgCdTe heterostructure measured at 80 K for different voltage bias.
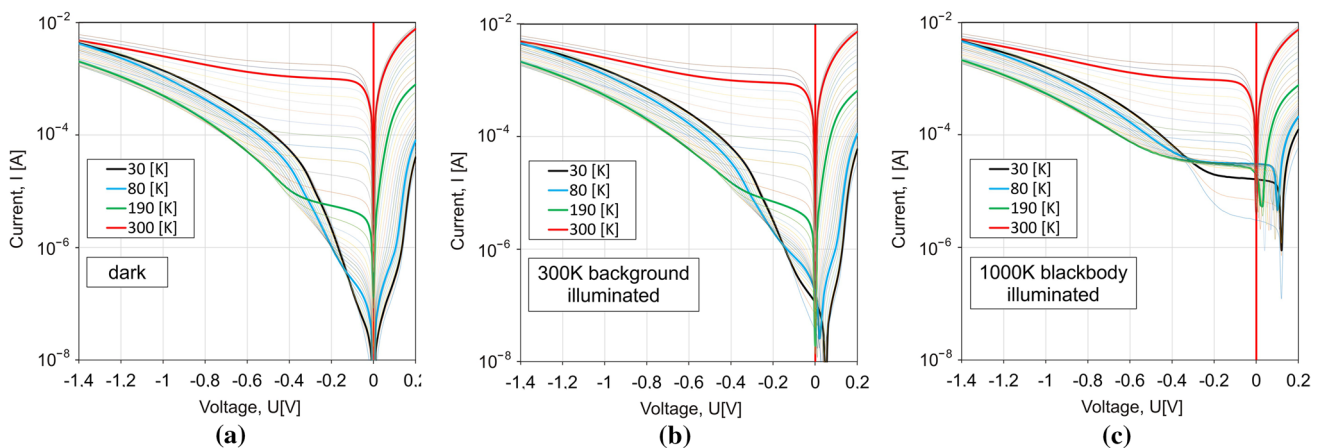
Fig. 4 Current–voltage characteristics of the $n^+G_3P^+G_2pG_1N^+$ HgCdTe heterostructure measured at different temperatures and conditions: (a) dark, (b) 300 K background-illuminated and (c) 1000 K blackbody-illuminated.
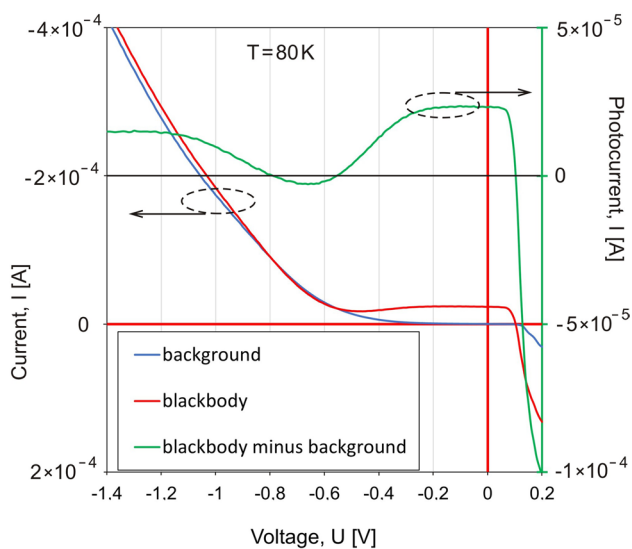
Fig. 6 Current–voltage characteristics of the $n^+G_3P^+G_2pG_1N^+$ HgCdTe heterostructure measured at 80 K with the photocurrent (the right axis)

Fig. 7 Temperature-dependent current–voltage characteristics (photocurrent originating only from the blackbody) of the $n^+G_3P^+G_2pG_1N^+$ HgCdTe heterostructure pictured in contour plot.

Results and Discussion

A comparison of the dark and illuminated (from the background and blackbody) current–voltage characteristics shown in Fig. 4a, b and c, respectively, enable us to isolate the photocurrent originating only from the blackbody. In this way, the contribution of the background can be eliminated. Figure 6 presents current–voltage characteristics measured at 80 K with an indication of the proportion of its individual components. The green line represents photocurrent originating only from the blackbody illumination. For the voltage range from about −0.55 V to about −0.8 V, the photocurrent changes direction. At a bias voltage below −0.8 V, the photocurrent becomes positive again, but its value is lower than the value at zero bias. The reflection of this effect can be seen in Fig. 5, where a negative signal appears at bias voltage of about −0.6 V in the vicinity of energy of about 530 meV, and then a large positive signal at a bias voltage below −0.8 V. This energy level corresponds to the absorption ability of the $Hg_{1-x}Cd_xTe$ material with composition of about $x = 0.48$. Looking at the structure project and its SIMS profile in Figs. 1 and 3, respectively, that photogeneration may take place at the N^+, G_1, G_2 or G_3 regions.

The contour maps concentrate a huge amount of data exposed in a single chart instead of presenting many 2D graphs. The temperature-dependent family of current–voltage characteristics (the photocurrent originating only from the blackbody radiation) of the $n^+G_3P^+G_2pG_1N^+$ HgCdTe heterostructure visualized in a contour plot are presented in Fig. 7. This graph shows the areas of negative values of the photocurrent (violet) that is flowing in the opposite direction
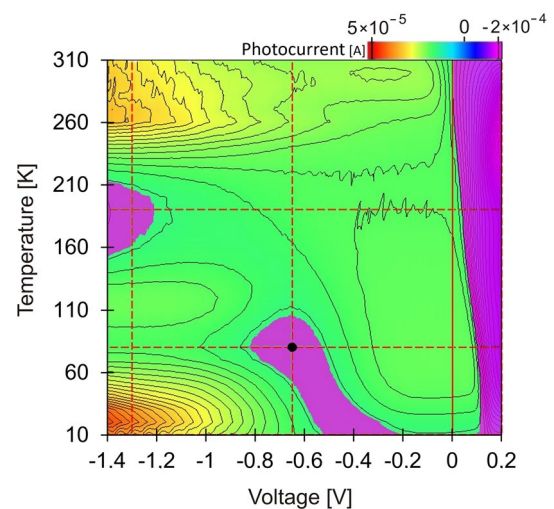
to the photocurrent originating from the absorber. The correlation between spectral and current–voltage characteristics measured with high resolution as a function of the temperature may indicate the origin of the signal, which is generated in the areas other than the absorber layer.

Spectral measurements of the detector response as a function of bias voltage were performed for selected temperatures. Figure 8 presents the relative response of the detector as a function of a bias voltage at temperatures of (a) 190 K, (b) 80 K, (c) 30 K and (d) 10 K, visualized as contour plots. The described phenomenon of the appearance of an additional signal source in certain reverse voltage ranges becomes more clearly visible at temperatures below 80 K. The signal relating to the energy of about 530 meV, which corresponds to a wavelength of about $\lambda = 2.4 \ \mu m$ for bias voltages from −0.4 V to −0.8 V, starts to dominate below 30 K (the red circular stain) and becomes even more apparent at 10 K. At the same temperatures, a second maximum appears at voltages below −0.8 V for a signal corresponding to energy of about 500 meV. Although the composition profile of the sample indicates N^+ as the origin of additional photocurrent, the direction of this component of the total photocurrent suggests that the G_3 region is equally likely for the location of the photogeneration at the bias voltage range from −0.4 V to −0.8 V. This signal does not disappear for voltages below −0.8 V, but is drowned out by the much larger signal coming from the G_1 layer. The continuation of studies on similar samples with theoretical result comparisons will allow for a more comprehensive understanding of this compound electronic material. Another solution to explain this phenomenon is to study a modified structure
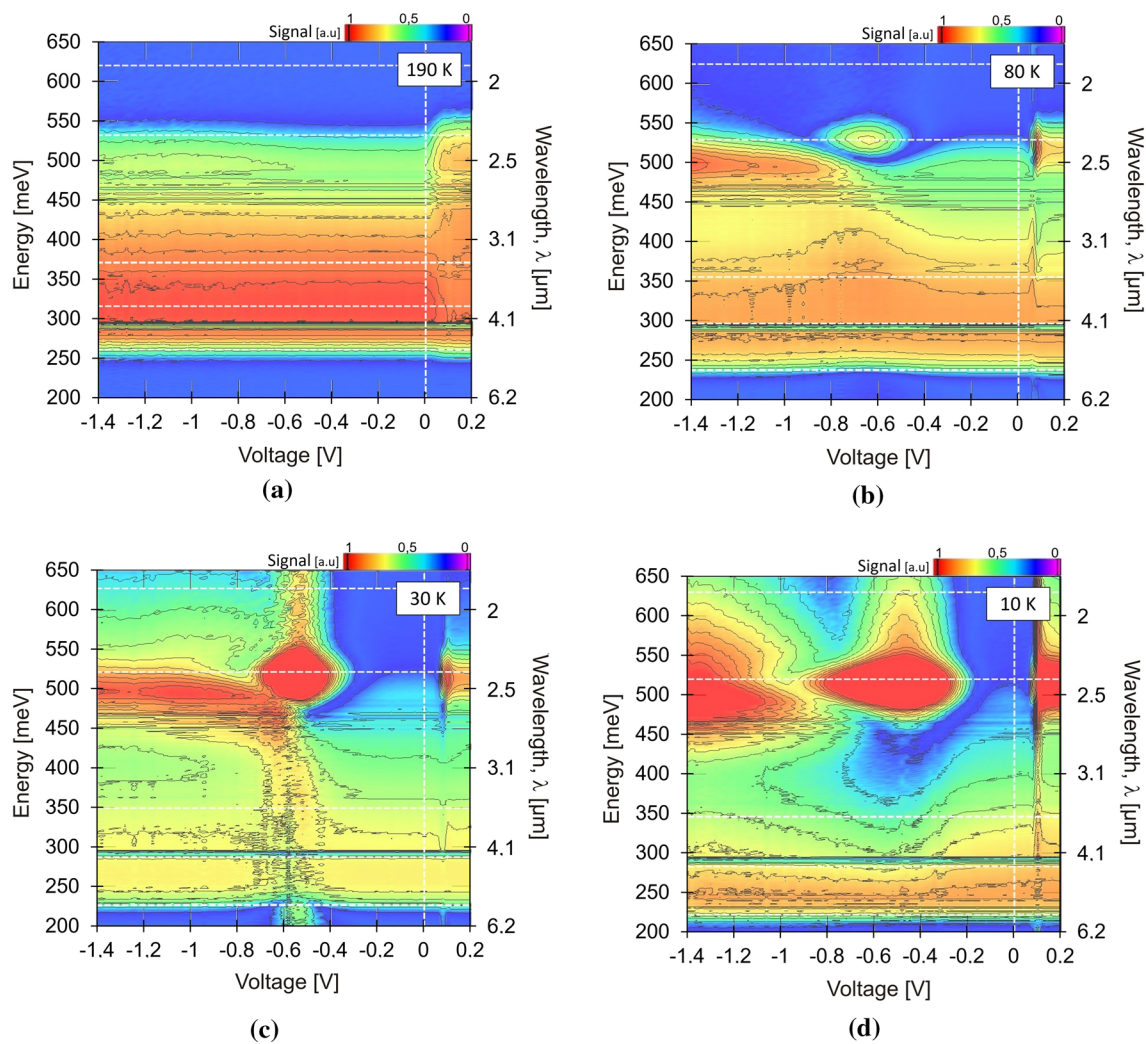
Fig. 8 Detector relative response as a function of a bias voltage for different temperatures of (a) 190 K, (b) 80 K, (c) 30 K and (d) 10 K pictured in contour plots.

in such a way as to illuminate the sample through the top contact (n^+).

Conclusions

The spectral response and current–voltage characteristics of a $n^+G_3P^+G_2pG_1N^+$ MWIR HgCdTe detector were studied. The MOCVD technique with a wide range of composition and donor/acceptor doping enables the growth of HgCdTe epilayers used for uncooled infrared detectors. Following the progress in the field of epitaxial growth, it is also necessary to develop characterization methods. The computer-controlled electronic analyzers with the support of LabVIEW enable multiple averaging of the measurement results and makes it possible to collect an enormous amount of data with high precision and high

resolution in a reasonable time, which was impossible with manual methods. The example of the automated correlation between current–voltage and spectral characteristics of the HgCdTe sample can help to extract the secondary components of the photocurrent and to find the location of its source. Such knowledge is indispensable in infrared detector designing and engineering.

Conflict of interest The authors declare no conflict of interest.

References

1. A. Rogalski, *Infrared and Terahertz Detectors* (New York: Taylor, 2018).

2. M. Kopytko and A. Rogalski, New insights into the ultimate performance of HgCdTe photodiodes. *Sens. Actuator A Phys.* (2022). https://doi.org/10.1016/j.sna.2022.113511.

3. C. Maxey, P. Capper, and I. Baker, MOVPE Growth of Cadmium Mercury Telluride and Applications, *Metalorganic Vapor Phase Epitaxy (MOVPE): Growth, Materials Properties, and Applications*. ed. S. Irvine, and P. Capper (New York: Wiley, 2019), pp. 293–324. https://doi.org/10.1002/9781119313021.ch9.

4. P. Mitra, F.C. Case, M.B. Reine, T. Parodos, S.P. Tobin, and P.W. Norton, MOVPE growth of HgCdTe for high performance 3–5 μm photodiodes operating at 100–180K. *J. Electron. Mater.* (1999). https://doi.org/10.1007/s11664-999-0040-z.

5. T.J. de Lyon, R.D. Rajavel, J.A. Roth, and J.E. Jensen, *Handbook of Infrared Detection and Technologies*. ed. by M. Henini, and M. Razeghi (Oxford: Elsevier, 2002), p. 309.

6. W.E. Tennant, C.A. Cockrum, J.B. Gilpin, M.A. Kinch, M.B. Reine, and R.P. Ruth, Key issues in HgCdTe-based focal plane arrays: an industry perspective. *J. Vac. Sci. Technol.* (1992). https://doi.org/10.1116/1.585869.

7. C.D. Maxey, J.P. Camplin, I.T. Guilfoy, J. Gardner, R.A. Lockett, C.L. Jones, P. Capper, M. Houlton, and N.T. Gordon, Metal-organic vapour-phase epitaxial growth of HgCdTe device heterostructures on three-inch-diameter substrates. *J. Electron. Mater.* (2003). https://doi.org/10.1007/s11664-003-0048-8.

8. P. Madejczyk, A. Piotrowski, W. Gawron, K. Kłos, J. Pawluczyk, J. Rutkowski, J. Piotrowski, and A. Rogalski, Growth and properties of MOCVD HgCdTe epilayers on GaAs substrates. *Opto-Electron. Rev.* 13, 59 (2005).

9. H. Nishino, S. Murakami, and Y. Nishijima, Structure and surface properties of metalorganic vapor phase epitaxial CdTe and HgCdTe(111)B layers grown on vicinal GaAs(100) subatrates. *J. Electron. Mater.* (1999). https://doi.org/10.1143/JJAP.38.5775.

10. W.S. Wang and I. Bhat, Materials science communication (100) or (111) heteroepitaxy of CdTe layers on (100) GaAs substrates by organometallic vapor phase epitaxy. *Mater. Chem. Phys.* (1997). https://doi.org/10.1016/S0254-0584(97)80290-8.

11. J. Tunnicliffe, S.J.C. Irvine, O.D. Dosser, and J.B. Mullin, A new MOCVD technique for the growth of highly uniform CMT. *J. Crystal Growth* 68, 245 (1984).

12. A. Piotrowski and K. Kłos, Metal-organic chemical vapor deposition of $Hg_{1-x}Cd_x$ Te fully doped heterostructures without post-growth anneal for uncooled MWIR and LWIR detectors. *J. Electron. Mater.* (2007). https://doi.org/10.1007/s11664-007-0171-z.

13. P. Madejczyk, W. Gawron, A. Kębłowski, D. Stępień, P. Martyniuk, A. Rogalski, J. Rutkowski, and J. Piotrowski, Higher operating temperature IR detectors of the MOCVD grown HgCdTe heterostructures. *J. Electron. Mater.* (2020). https://doi.org/10.1007/s11664-020-08369-3.

14. W. Gawron, J. Sobieski, T. Manyk, M. Kopytko, P. Madejczyk, and J. Rutkowski, MOCVD grown HgCdTe heterostructures for medium wave infrared detectors. *Coatings* (2021). https://doi.org/10.3390/coatings11050611.